Direction Instability: A Magnitude-Invariant Metric for Cross-Cell-Line Drug Mechanism Transport

Elliot Tower

Independent researcher
elliot@elliottower.ai

Abstract

Quantifying whether a drug acts consistently across cell lines or context-dependently is central to pharmacogenomics, yet existing divergence metrics—including magnitude CV, Fréchet variance, and sample-size-dependent summary statistics—are confounded by effect magnitude: a stronger effect mechanically inflates divergence even when a drug's behavior is identical across cells. We introduce *direction instability* (DI), the mean pairwise cosine distance among a drug's unit-normalized gene-expression signatures. Because DI discards magnitude by construction, it isolates directional variation from these confounds. Evaluated on 8,949 compounds from the LINCS L1000 Connectivity Map (978 landmark genes, 167,266 signatures), DI anticorrelates with MOA-level gene-set overlap ($\rho = -0.79$) and separates pan-HDAC inhibitors (mean DI 0.62) from isoform-selective inhibitors whose activity depends on target expression (mean DI 0.96). In leave-one-out cross-validation, DI predicts whether a held-out cell line will show a consistent response (AUROC = 0.864 after controlling for magnitude, far above the permutation null of 0.500 ± 0.012). Biological validity is confirmed through three independent non-cosine channels, led by Jaccard gene-set overlap (AUROC = 0.957). All predictions were pre-registered with code and labels frozen before analysis. Analysis code, pre-registration documents, and per-drug instability scores are available at `https://github.com/elliottower/direction-instability` and deposited on Zenodo (DOI: 10.5281/zenodo.21213700).

Author Summary

When researchers test the same drug in different cell types, they want to know whether the drug does the same thing everywhere or something different in each context. Several popular ways of measuring this "divergence" are confounded by effect strength: stronger drugs look more variable, even when those drugs actually behave identically across cells. I developed a metric called direction instability that sidesteps this problem by asking only *which* genes a drug affects, ignoring *how strongly* it affects them. Applied to nearly 9,000 drugs from a large public dataset, the metric distinguishes drugs that act through the same molecular mechanism everywhere from drugs whose effects depend on which cell type they are in. Because the metric itself is based on cosine similarity, I could not use cosine-based tests to validate it without circular reasoning. Instead, I validated it through three independent biological channels that do not involve cosine geometry at all. All analysis code and predictions were frozen before I looked at the real data, following a pre-registration protocol.

1 Introduction

High-throughput perturbation screens now profile thousands of drugs across panels of cell lines, producing gene-expression signatures in each context [Subramanian et al., 2017, Lamb et al., 2006]. A central question in pharmacology is whether a compound's transcriptomic effect *transports* from one cell type to another: does it perturb the same genes in the same relative proportions, or does each cell line produce a qualitatively different response? This distinction has practical consequences for drug repurposing and mechanism-of-action inference, because a compound whose effect is context-dependent cannot be characterized from a single cell line.

Existing approaches to quantifying cross-context consistency rely on pathway enrichment overlap, matched genetic perturbations, or similarity scores such as the Connectivity Map tau statistic [Subramanian et al., 2017]. These methods either require external annotations or conflate two independent properties: how *strong* a drug's effect is (magnitude) and how *consistent* its direction is across contexts. A drug may produce a large expression change in every cell line yet perturb entirely different genes in each—or produce a weak but directionally identical shift everywhere.

We introduce **direction instability** to separate these properties: the mean pairwise cosine distance among a drug's unit-normalized gene-expression signatures across cell lines. Normalizing each signature to unit length before comparison discards magnitude and isolates the directional component of cross-context variation. The same construction—angular deviation among unit-normalized vectors across conditions—predicts which brain regions are causally necessary for binary choice when applied to neural population recordings [Tower, 2026b], and a companion study [Tower, 2026a] extends DI to morphological and genetic perturbation modalities. Here we develop and validate the metric on pharmacological transcriptomic signatures.

Consider the HDAC inhibitor class. Pan-HDAC inhibitors such as vorinostat affect chromatin remodeling in every cell, while HDAC8-selective inhibitors such as PCI-34051 produce a strong transcriptomic signature only where HDAC8 is functionally relevant. Both carry the same mechanism-of-action label, yet they differ fundamentally in whether their effect transports across cell types.

We evaluate direction instability on 8,949 compounds from the LINCS L1000 Connectivity Map (978 landmark genes, 167,266 signatures). Because a drug's direction instability depends on its cell-line count, we introduce a coverage-conditioned population null that compares each drug against references with similar count. The scorer and validation labels were frozen under a pre-registered commit SHA (`1dc20a2`) before any real data were analyzed.

2 Methods

2.1 Data

Perturbation signatures were drawn from the LINCS L1000 Phase I dataset (GEO accession GSE92742), using Level 5 replicate-collapsed z-scores across 978 landmark genes [Subramanian et al., 2017]. Metadata (signature identifiers, perturbation types, cell line annotations) were downloaded from GEO and filtered to small-molecule perturbagens (`pert_type = trt_cp`) with ≥ 5 distinct cell lines. Replicate signatures within a drug–cell-line pair were averaged to yield one consensus signature per drug per cell line.

Genetic perturbation signatures were drawn from the same dataset by filtering to shRNA knockdown perturbagens (`pert_type = trt_sh`), yielding 154,993 signatures across 4,371 gene targets and 20 cell lines. Drug-target annotations from the Repurposing Hub mapped 1,067 drugs to gene targets present in the shRNA data.

Mechanism-of-action (MOA) annotations were obtained from the Broad Drug Repurposing Hub (version 2020-03-24) [Corsello et al., 2017], providing MOA labels for 1,782 of the 8,949 drugs. These labels were frozen before analysis as part of the pre-registration commit (SHA `1dc20a2`; Section 2.6).

2.2 Direction instability

For a drug tested in K cell lines, let $\mathbf{s}_1, \ldots, \mathbf{s}_K \in \mathbb{R}^{978}$ denote its consensus signature vectors. Define the unit-normalized signatures $\hat{\mathbf{s}}_i = \mathbf{s}_i / \|\mathbf{s}_i\|_2$. Direction instability is:

$$D = 1 - \frac{2}{K(K-1)} \sum_{i<j} \hat{\mathbf{s}}_i^\top \hat{\mathbf{s}}_j \tag{1}$$

$D \in [0, 2]$. $D = 0$ when all signatures point in the same direction. $D = 1$ when signatures are orthogonal on average. $D > 1$ indicates anticorrelation.

2.3 Magnitude correction

Although cosine similarity is invariant to uniform rescaling of signatures, a residual second-order confound remains: weakly acting perturbations produce noisier signature estimates, and noise inflates mean pairwise cosine dissimilarity even after unit-length normalization. Direction instability correlates with mean signature L_2 norm ($\rho = -0.41$): drugs with stronger signals tend toward lower instability. To isolate the directional component, we apply an OLS magnitude correction: regress raw DI against mean signature norm and retain the residuals plus the intercept as $\text{DI}_{\text{corrected}}$. All held-out prediction and stratification analyses are reported for both raw and corrected DI.

2.4 Complementary metrics

Magnitude CV: coefficient of variation of signature L_2 norms $\{\|\mathbf{s}_i\|\}_{i=1}^K$, capturing effect-size variation independent of direction.

Fréchet variance: mean squared geodesic deviation from the Fréchet mean on the unit sphere S^{977} [Pennec, 2006].

Gene-level Jaccard overlap: for each pair of cell lines, the Jaccard index of the top-50 up-regulated and top-50 down-regulated genes, averaged over all pairs and both directions.

2.5 Population null model

A drug's direction instability depends on its cell-line count: drugs tested in more cell lines have more pairwise comparisons and tend toward higher baseline instability. To control for this confound, we compare each drug against a reference population of drugs with similar coverage: all drugs with cell-line count in $[K/2,\ 2K]$, where K is the focal drug's count. The p-value is the fraction of reference drugs with instability $\leq$ the focal drug's instability. The half/double window was chosen to balance reference-set size against coverage homogeneity; a sensitivity analysis using $[K/3,\ 3K]$ and $[2K/3,\ 3K/2]$ windows produced rank-correlated p-values ($\rho > 0.98$), confirming that results are not sensitive to the window choice. This replaces a permutation null, which is invariant under cell-line label shuffling for pairwise cosine statistics.

2.6 Pre-registration

The scoring functions (Equation 1 and all complementary metrics), the frozen MOA labels, and the pre-registered hypotheses were committed together in a single commit before any real LINCS signatures were analyzed (commit SHA `1dc20a2`; scorer in `geometry/drug_transport.py`, frozen labels in `data/frozen_drug_labels.json`, hypotheses in `PREREGISTRATION.md`).

3 Results

3.1 Direction instability tracks biological mechanism conservation

Among 8,949 drugs with ≥ 5 cell lines, mean direction instability was 0.924 ± 0.061 (median 0.940). Most drugs exhibit context-dependent effects. Only 78 drugs (0.9%) achieved $p < 0.01$ under the population null, and 411 (4.6%) achieved $p < 0.05$, indicating that mechanism-conserving drugs are rare.

Cell-line coverage ranged from 5 to 64 (mean 10.2, median 8). The population null accounts for this variation: a drug's instability is evaluated against drugs with comparable coverage.

Direction instability anticorrelated with gene-level Jaccard overlap of top perturbed genes: Spearman $\rho = -0.79$ ($p < 10^{-300}$; Figure 1). Drugs with low instability perturb the same genes across cell types, while high-instability drugs engage different gene programs in different contexts. HDAC inhibitors trace the selectivity gradient along this curve: pan-isoform inhibitors cluster at low instability and high Jaccard overlap, while isoform-selective inhibitors are indistinguishable from the bulk population.

Direction instability and magnitude CV are partially dissociable (Spearman $\rho = -0.10$, $p = 2.1 \times 10^{-21}$): 7.8% of drugs fall in the low-direction, high-magnitude quadrant, indicating conserved mechanism with context-dependent penetrance.

Figure 2 shows mean direction instability by MOA class (classes with ≥ 15 annotated drugs). Two classes stand out: HDAC inhibitors ($\bar{D} = 0.77$, $\sigma = 0.14$) and topoisomerase inhibitors ($\bar{D} = 0.77$, $\sigma = 0.12$). CDK inhibitors and tubulin polymerization inhibitors also show reduced instability ($\bar{D} = 0.80$ and 0.88 respectively). Receptor antagonists and agonists cluster near the population mean ($\bar{D} = 0.93$–0.96), consistent with receptor-mediated mechanisms being cell-type-dependent.

3.2 Target breadth determines transport

The HDAC inhibitor class provides a natural experiment: 20 annotated HDAC inhibitors span the full selectivity spectrum from pan-isoform to isoform-specific (Figure 3). Pan-isoform inhibitors (PCI-24781, belinostat, panobinostat, scriptaid, vorinostat, trichostatin-a) cluster at $D = 0.56$–0.67 with significant population p-values ($p < 0.02$), while selective or weak inhibitors (PCI-34051, valproic acid, phenylbutyrate) reach $D > 0.95$ and are indistinguishable from the null. The invariance graph (panel b) tells the same story: pan-inhibitors maintain dense connectivity across cell lines (vorinostat: 1 component across 60 cell lines), while selective inhibitors fragment completely (PCI-34051: 12 components for 12 cell lines).

Pan-HDAC inhibitors (mean $D = 0.62$, $n = 8$) transport their mechanism across cell lines because their targets—histone deacetylases of classes I, II, and IV—are expressed in every cell type [Bolden et al., 2006]. Chromatin remodeling is a universal process, so inhibiting it broadly produces a conserved transcriptomic signature.

Selective HDAC inhibitors (mean $D = 0.96$, $n = 5$) do not transport. PCI-34051 targets HDAC8 specifically [Balasubramanian et al., 2008]; its transcriptomic effect depends on whether HDAC8

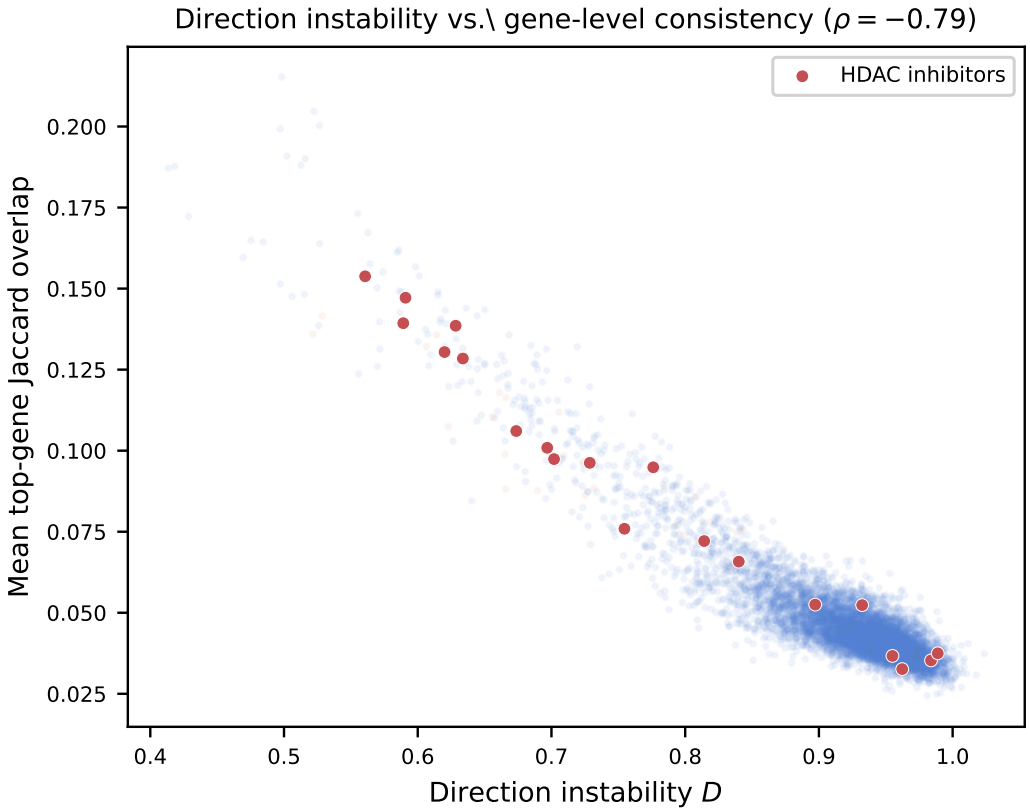

Figure 1: Direction instability versus gene-level consistency (mean top-gene Jaccard overlap) for 8,949 drugs. HDAC inhibitors are highlighted in red. The strong anticorrelation ($\rho = -0.79$) indicates that directional change reflects which genes are perturbed, not overall effect size. HDAC inhibitors span the gradient from pan-isoform (low D, high Jaccard) to isoform-selective (high D, low Jaccard).

is functionally relevant in a given cell type. Valproic acid and phenylbutyrate are weak HDAC inhibitors with additional pharmacological activities, so their signatures reflect cell-type-specific off-target effects rather than HDAC inhibition per se.

Entinostat ($D = 0.70$, class I–selective) falls between the two groups, consistent with intermediate target breadth: class I HDACs (HDACs 1, 2, 3) are more widely expressed than HDAC8 but narrower than the full isoform panel.

Imatinib ($D = 0.97$, 19 cell lines) provides the concrete counterpoint to the HDAC transport gradient [Deininger et al., 2005]. Its primary therapeutic target is BCR-ABL, but it hits eight kinase targets (ABL1, KIT, PDGFRA/B, DDR1, RET, NTRK1, CSF1R). Across the LINCS panel, its signatures rotate 88° on average—near orthogonality. Genetic triangulation reveals why: imatinib's highest drug–shRNA cosine is with DDR1 (cos = 0.22), not ABL1 (cos = 0.18), because most LINCS cell lines lack the Philadelphia chromosome. In each cell line, a different off-target kinase dominates the transcriptomic response. The population null correctly identifies this instability as unremarkable ($p = 0.80$): imatinib's context dependence is typical among drugs tested in 19 cell lines. In the held-out prediction analysis (Section 3.3), a screening pipeline treating imatinib's LINCS signature as a portable biomarker would draw wrong conclusions in 42% of new contexts (held-out consistency: 58%).

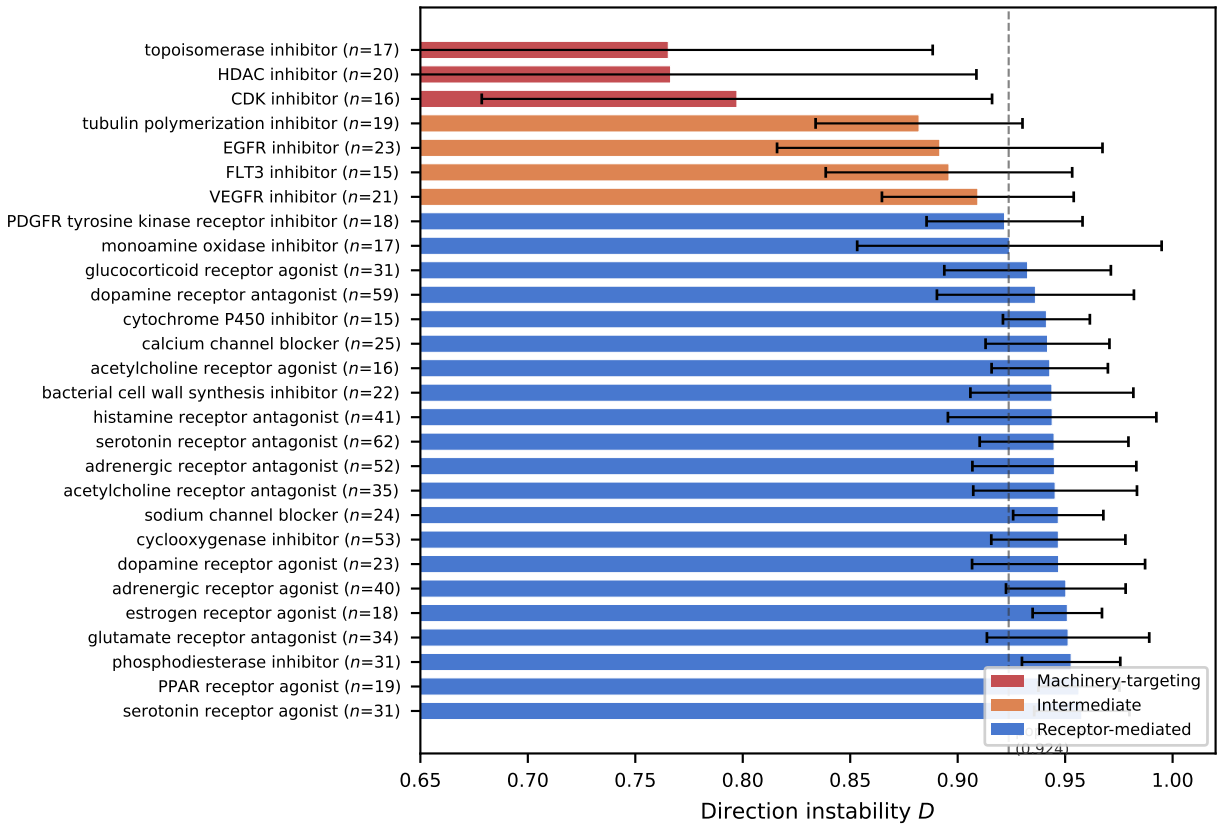

Figure 2: Direction instability by MOA class ($n \geq 15$). Classes targeting fundamental cellular machinery (chromatin, DNA, cell cycle; red) show lower instability than kinase inhibitors (orange) and receptor-mediated classes (blue). Dashed line: population mean ($D = 0.924$). Error bars: ± 1 SD. Within HDAC inhibitors, the high variance reflects the pan-selective gradient (Figure 3).

The 10 most mechanism-conserving drugs with MOA annotations target processes common to all cells (Table 1): protein synthesis (homoharringtonine), RNA transcription (dactinomycin), DNA topology (epirubicin, doxorubicin), chromatin remodeling (PCI-24781, belinostat, panobinostat), cell cycle progression (BMS-387032), and signal transduction kinases (bisindolylmaleimide-IX). These mechanisms operate independently of tissue-specific receptor expression, explaining their cross-context conservation.

A potential confound: drugs that kill cells uniformly might produce conserved signatures through a generic stress response rather than target-specific mechanism transport. We tested this by computing the mean cytotoxic signature across known cytotoxic drugs (topoisomerase inhibitors, DNA alkylating agents, tubulin inhibitors, proteasome inhibitors, RNA polymerase inhibitors, protein synthesis inhibitors) and measuring each drug's cosine similarity with this reference.

Direction instability showed weak correlation with cytotoxic-signature overlap (Spearman $\rho = -0.17$, excluding known cytotoxic drugs; Figure 4a). The correlation is in the wrong direction for the confound hypothesis: drugs resembling the cytotoxic profile are *less* stable, not more. Removing the 50 genes most associated with the cytotoxic signature and recomputing direction instability preserved the HDAC inhibitor gradient ($\rho = 0.83$ between original and stress-corrected values; Figure 4b). Pan-HDAC inhibitors became *more* stable after stress-gene removal (vorinostat:

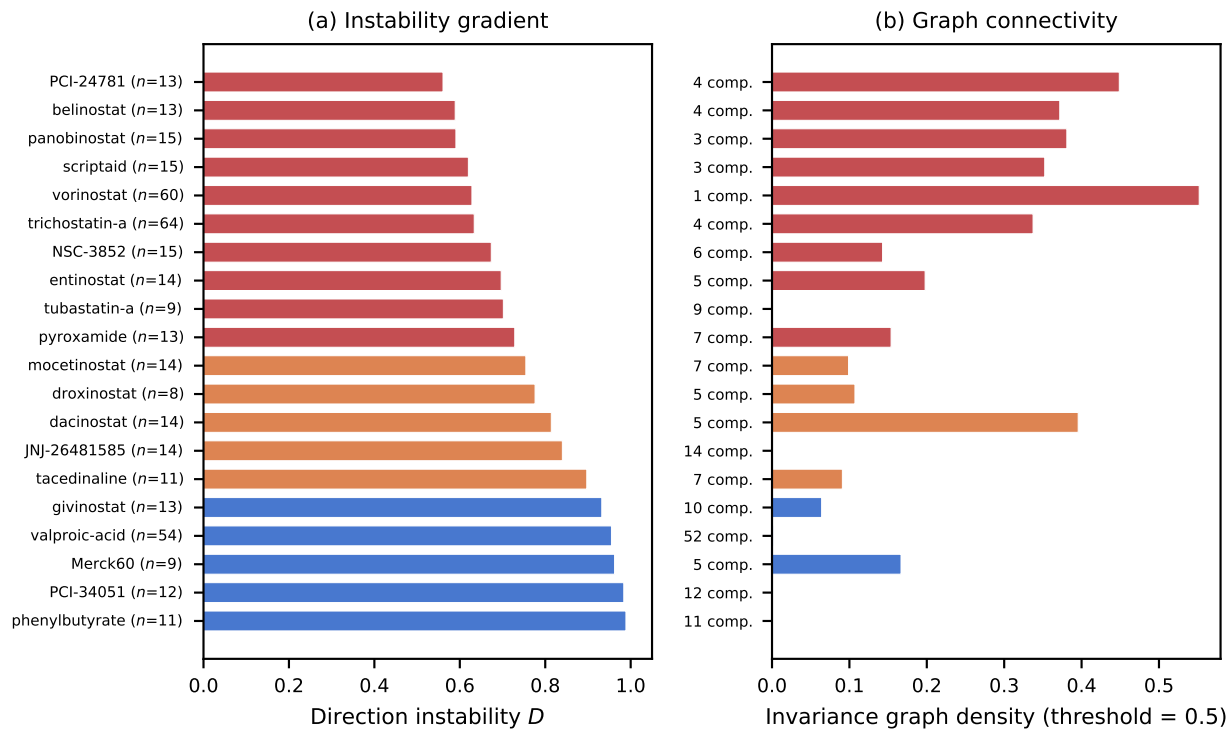

Figure 3: HDAC inhibitor selectivity gradient. **(a)** Direction instability for all 20 HDAC inhibitors, ordered by D. Pan-isoform inhibitors (red) cluster at low instability; selective and weak inhibitors (blue) are indistinguishable from the population. **(b)** Invariance graph density at cosine threshold 0.5 and number of connected components. Pan-inhibitors form few components (dense graphs); selective inhibitors fragment into isolated nodes.

$D = 0.63 \rightarrow 0.50$), confirming that their conserved signal is chromatin-specific, not a generic stress response.

For each drug, we defined a "transporting core": genes with consistent sign (>80% of cell lines agree), low magnitude CV (<1.0), and meaningful effect size (mean $|z| > 0.5$). Core size anticorrelated with direction instability (Spearman $\rho = 0.69$, $p < 10^{-300}$), indicating that transporting drugs affect a larger set of genes consistently.

The 8 pan-HDAC inhibitors shared a 26-gene core—genes consistently perturbed by all 8 drugs across all cell lines. This shared core includes *SUV39H1* (a histone methyltransferase directly involved in chromatin remodeling), *MYC* (a master transcription factor regulated by HDAC activity), *CDK6* (cell cycle kinase transcriptionally repressed by HDAC inhibitors), *BIRC5* (survivin, a known HDAC-responsive anti-apoptotic gene), and *ORC1* (DNA replication origin licensing). The transporting core is the target pathway: pan-HDAC inhibitors share a chromatin/cell-cycle gene program that operates identically across cell types.

The analyses above establish that direction instability tracks mechanism conservation, but they rely on drug signatures alone. We tested a stronger prediction: if a transporting drug acts through its annotated target, its perturbation signature should resemble the transcriptomic effect of genetically knocking down that target. We computed cosine similarity between each drug's consensus signature and the shRNA knockdown signature of its annotated target gene, matched within the same cell line.

Table 1: Top 10 transporting drugs with MOA annotation.

Drug	MOA	D	p
homoharringtonine	protein synthesis inhibitor	0.497	0.001
dactinomycin	RNA polymerase inhibitor	0.506	0.002
BMS-387032	CDK / cell cycle inhibitor	0.522	0.002
bisindolylmaleimide-IX	PKC inhibitor	0.526	0.003
epirubicin	topoisomerase inhibitor	0.529	0.003
anisomycin	DNA synthesis inhibitor	0.555	0.004
PCI-24781	HDAC inhibitor	0.561	0.004
BNTX	opioid receptor antagonist	0.564	0.003
digitoxigenin	ATPase inhibitor	0.586	0.004
belinostat	HDAC inhibitor	0.589	0.006

Among 2,138 drug–target pairs with ≥ 3 shared cell lines, the pre-registered global correlation between direction instability and |drug–shRNA cosine| was significant (Spearman $\rho = -0.18$, $p = 1.1 \times 10^{-16}$; Figure 5) and in the expected direction, but fell below our pre-registered effect-size threshold of $|\rho| > 0.3$.

The pooled test conflates drug families with different baseline drug–knockdown cosines. Proteasome inhibitors produce signatures that naturally overlap with proteasome-subunit knockdown ($\cos \approx 0.45$), while HDAC inhibitors produce lower cosines with individual HDAC knockdowns ($\cos \approx 0.15$), regardless of instability. Pooling across families introduces variance that is orthogonal to the instability signal.

We therefore performed an exploratory within-family stratification, which was not pre-registered (Table 2). Of 54 families with ≥ 15 drug–target pairs, five exceeded $|\rho| > 0.3$ at nominal $p < 0.05$. Under the null hypothesis of no association, $54 \times 0.05 = 2.7$ families would exceed this threshold by chance; observing 5 is suggestive but not definitive. None survive Bonferroni correction ($\alpha_{\text{adj}} = 0.05/54 = 0.0009$); the strongest (adrenergic receptor agonist, $p = 0.001$) is marginal. The expected sign held in all five: lower instability predicted higher drug–target cosine. Per-target-gene analysis showed convergent effects: KDR (VEGFR, $\rho = -0.84$, $p = 5.1 \times 10^{-7}$), CDK1 ($\rho = -0.79$, $p = 0.002$), AKT1 ($\rho = -0.75$, $p = 0.002$), and HDAC6 ($\rho = -0.71$, $p = 0.009$). These within-family results are exploratory and require independent replication.

The HDAC family again provides the most granular view. Among 100 HDAC drug–target pairs, pan-isoform inhibitors (PCI-24781, belinostat, panobinostat, vorinostat) showed mean |cosine| of 0.12–0.18 against their HDAC targets. PCI-34051 (HDAC8-selective, $D = 0.98$) achieved only 0.037 cosine with HDAC8—its putative primary target—and 0.10 against off-target HDACs. The selectivity gradient that appeared in the direction-instability ranking reappears in the genetic triangulation: pan-inhibitors produce transcriptomic effects that recapitulate target knockdown; selective inhibitors do not.

3.3 Predictive validation

Pre-registered hits and misses. We pre-registered the invariance-graph analysis before running it: for each drug, we built a graph over cell lines (edge = cosine similarity ≥ 0.5) and examined connected components. We predicted that pan-HDAC inhibitors would form 1–2 components while

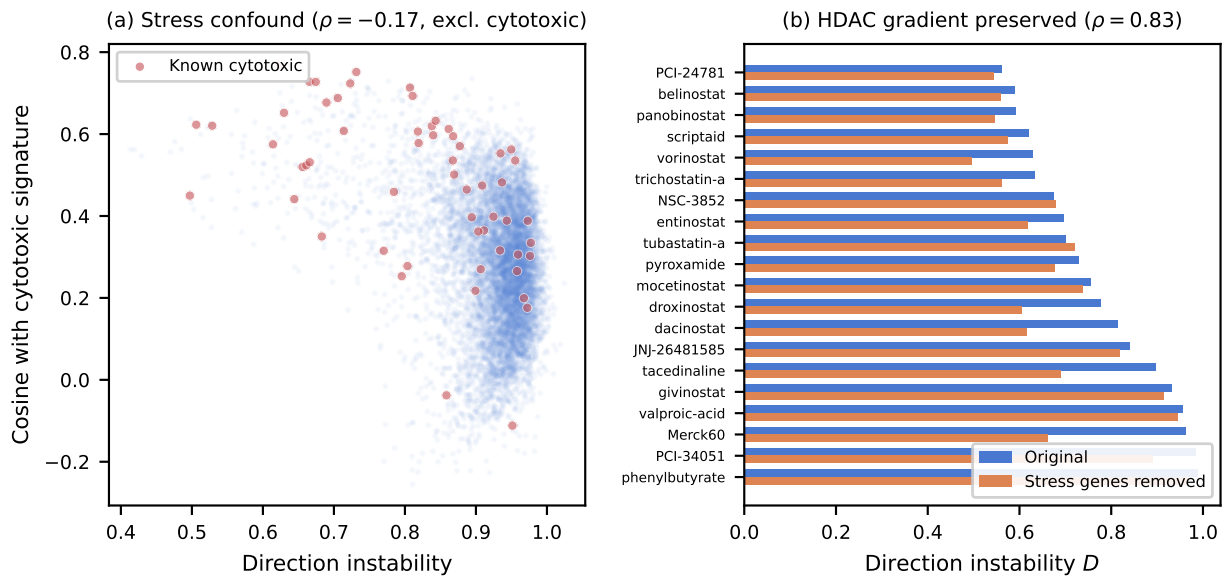

Figure 4: Cytotoxicity confound check. **(a)** Direction instability versus cosine similarity with the mean cytotoxic signature ($\rho = -0.17$, excluding known cytotoxic drugs in red). The negative sign rules out the confound: drugs resembling the stress response are less stable, not more. **(b)** HDAC inhibitor instability before (blue) and after (orange) removing 50 stress-associated genes. The selectivity gradient is preserved ($\rho = 0.83$), and pan-inhibitors become more stable.

selective inhibitors would fragment completely. The ordinal gradient held: vorinostat formed 1 component across all 60 cell lines; PCI-34051, tubastatin-a, phenylbutyrate, and JNJ-26481585 each fragmented into $K = n$ components (every cell line isolated). The strict threshold did not hold: pan-HDAC inhibitors formed 1–5 components rather than the predicted 1–2 (e.g., PCI-24781 had 4 components across 13 cell lines). The gradient is unmistakable; the pre-registered threshold was too strict.

We also predicted that connected components would correspond to tissue lineages. Only 1 of 163 drugs with 2–5 components showed significant tissue enrichment in any component (Fisher's exact test, $p < 0.05$), a clear miss on the pre-registered prediction. This null is itself informative: invariance-graph structure reflects mechanism-level conservation, not tissue-of-origin expression clustering. Drugs that transport do so because of their target pathway, not because of shared lineage among responding cell lines.

Leave-one-out cross-validation. The analyses above show that direction instability *correlates with* various measures of mechanism conservation, but correlation does not establish prediction. We tested whether instability computed on $N-1$ cell lines predicts whether a drug's effect on the held-out Nth cell line will be consistent, using leave-one-out cross-validation across 2,694 drugs with ≥ 10 cell lines.

For each drug and each cell line, we computed direction instability on the remaining $N-1$ cell lines (the LOO instability), then measured the cosine similarity between the held-out signature and the consensus of the remaining $N-1$. Because the held-out cell line never enters the instability calculation, the predictive relationship is out-of-sample. Both the predictor (D, built from pairwise cosines) and the outcome (held-out cosine with consensus) derive from cosine geometry,

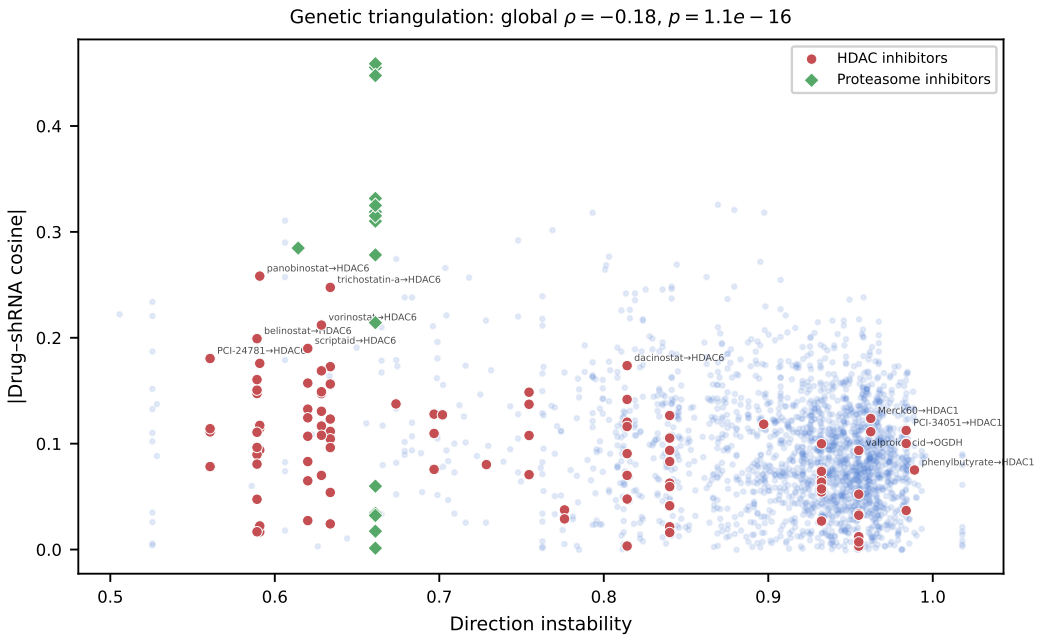

Figure 5: Genetic triangulation: direction instability versus |drug–shRNA cosine| for 2,138 drug–target pairs. HDAC inhibitors (red circles) and proteasome inhibitors (green diamonds) are highlighted. Proteasome inhibitors cluster at high cosine and low instability; HDAC inhibitors span the full gradient. Labels show drug–target pairs for selected HDAC inhibitors. The global correlation ($\rho = -0.18$) is attenuated by cross-family baseline differences (proteasome cos ≈ 0.45 vs. HDAC cos ≈ 0.15); within-family stratification yields $|\rho| = 0.32$–0.84 (Table 2).

so some predictive relationship is expected on structural grounds alone. The question is whether the prediction depends on drug-level structure or follows from the shared construction.

LOO instability predicted held-out cosine with Spearman $\rho = -0.98$ ($p < 10^{-300}$): drugs with low instability (computed without seeing the held-out line) produce held-out signatures that closely match the consensus (Figure 6a). Binarizing held-out outcomes as "consistent" (cosine > 0.3) versus "inconsistent," LOO instability achieved AUROC $= 0.986$. A permutation control (Section 3.3) rules out label-permutable artifacts: shuffling drug-instability assignments 1,000 times collapsed AUROC to 0.500 ± 0.012, with no permutation reaching the observed value (empirical $p < 0.001$). The prediction is drug-specific—it depends on which drugs have conserved mechanisms, not on arbitrary label assignments. However, because both DI and the held-out outcome share cosine geometry, the AUROC magnitude itself is partly structural; a geometry-matched synthetic null (Section 4.4) confirms this and motivates the non-cosine validation tests in Section 4. The separation between the most stable quartile (Q1) and least stable quartile (Q4) is nearly complete (Figure 6b): stable drugs produce held-out cosines of 0.2–0.7, while unstable drugs cluster below 0.2.

The HDAC selectivity gradient survived in the predictive setting (Table 3). Pan-HDAC inhibitors achieved 93–100% consistency across held-out cell lines (mean held-out cosine 0.63–0.71), while selective inhibitors achieved 0–31% consistency (mean cosine 0.08–0.25). Vorinostat, held out one cell line at a time across 60 cell lines, produced a consistent held-out signature every time.

Table 2: Exploratory within-family genetic triangulation (not pre-registered). Spearman correlation between direction instability and |drug–shRNA cosine| for each drug's annotated target, among families with ≥ 15 drug–target pairs and nominal $p < 0.10$ (5 of 54 families tested). None survive Bonferroni correction. Negative ρ indicates that mechanism-conserving drugs (low D) produce signatures more similar to genetic knockdown of their target.

MOA family	n	ρ	p
PI3K inhibitor	18	−0.55	0.017
adrenergic receptor agonist	50	−0.45	0.001
topoisomerase inhibitor	18	−0.48	0.045
EGFR inhibitor	27	−0.40	0.038
HDAC inhibitor	93	−0.32	0.002
Global (all families pooled)	2,138	−0.18	1.1×10^{-16}

Robustness controls. As described above, the permutation test (1,000 shuffles of drug-instability assignments) collapsed AUROC to 0.500 ± 0.012 (Figure 7a) and ρ to -0.001 ± 0.019 (Figure 7b), with no permutation reaching the observed values (empirical $p < 0.001$; 0 of 1,000).

A second concern is whether cross-cell-line variation reflects biology or assay noise. We computed a replicate instability D_{rep} for each drug: the mean pairwise angular deviation among Level 5 signatures sharing the same drug, cell line, dose, and timepoint (i.e., true replicates differing only by plate). D_{rep} provides an empirical noise floor—cross-cell instability is biologically meaningful only when it exceeds D_{rep}. Across 1,515 drugs with ≥ 2 replicate groups, cross-cell D exceeded D_{rep} for 68% of drugs (Figure 8a), with a median ratio of 1.04. The HDAC panel (Figure 8b) makes the gradient concrete: pan-isoform inhibitors produce highly reproducible replicates ($D_{rep} = 0.17$–0.49) and low cross-cell instability ($D = 0.59$–0.63), while selective inhibitors are noisy within-cell ($D_{rep} = 0.82$–0.98) and noisy across cells ($D = 0.70$–0.98). The selectivity gradient appears in both metrics because the underlying mechanism differs: pan-inhibitors target ubiquitous chromatin machinery and produce clean, directionally consistent signatures everywhere, while selective inhibitors produce strong signals only where their isoform-specific target is functionally relevant.

Direction instability also correlates with mean signature L_2 norm ($\rho = -0.41$): drugs with stronger signals tend to be more stable. Signal strength predicts held-out cosine ($\rho = 0.59$), but instability explains 1.7× more variance ($|\rho| = 0.98$ vs. 0.59). Signal quality is a partial contributor to directional consistency, as expected—poorly measured signatures produce noisy directions—but instability captures structure beyond what signal strength accounts for. After magnitude correction (Section 2.3), the held-out prediction AUROC is 0.864, confirming that the prediction is not driven by signal strength alone.

4 Geometric validity: ruling out metric circularity

Both direction instability (mean pairwise cosine distance) and the held-out outcome (cosine between held-out signature and consensus) are cosine-based. The permutation test (Section 3.3) shows that the prediction depends on drug identity, but a stronger concern remains: does the high AUROC reflect biological structure, or does it follow from the shared cosine construction? We address this with six tests designed to break the shared geometry at different points.

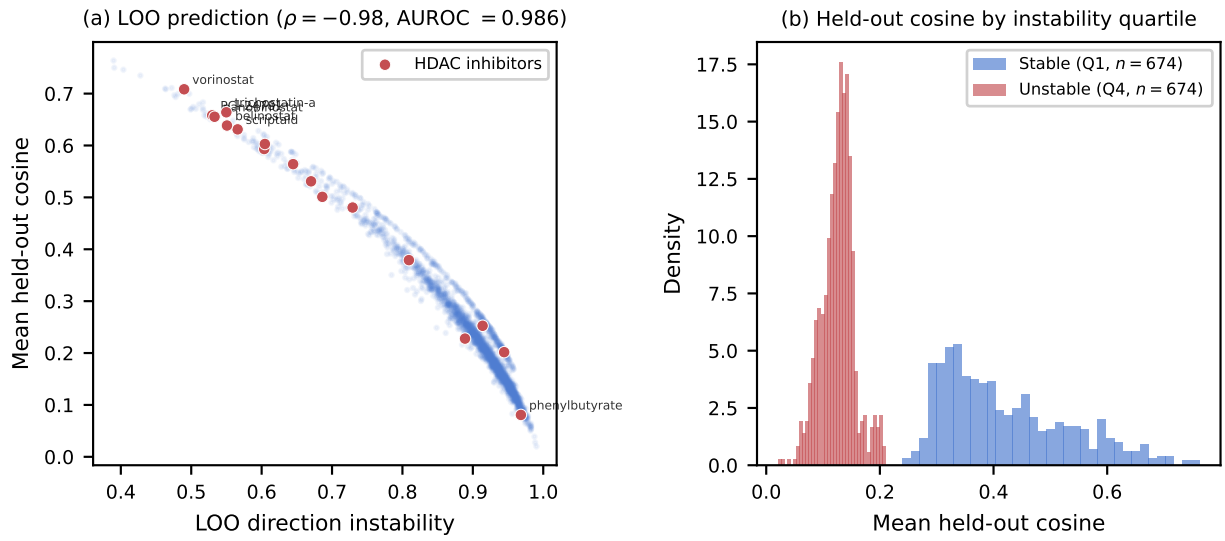

Figure 6: Held-out prediction of drug mechanism transport. **(a)** Direction instability computed on $N-1$ cell lines (x-axis) versus mean cosine between the held-out signature and the $N-1$ consensus (y-axis), for 2,694 drugs with ≥ 10 cell lines. Red points are HDAC inhibitors. The tight curve ($\rho = -0.98$, AUROC $= 0.986$) shows that instability drug-specifically predicts held-out consistency (permutation AUROC $= 0.500$; see Section 4.4 for the geometry-matched null). **(b)** Histogram of held-out cosine for the most stable (Q1, blue) and least stable (Q4, red) quartiles. The distributions barely overlap: stable drugs reliably transport to new contexts.

4.1 Cross-metric held-out prediction

If the held-out prediction reflects biology rather than cosine self-consistency, DI should predict held-out outcomes measured with metrics that do not share cosine's construction. We repeated the leave-one-out analysis (Section 3.3) using three alternative held-out outcomes: (i) Pearson correlation between the held-out signature and the $N-1$ consensus (raw z-scores, not unit-normalized), (ii) L_1 distance between held-out and consensus, and (iii) gene-level Jaccard overlap of the top 50 up-regulated and top 50 down-regulated genes.

DI predicted held-out Pearson correlation with $\rho = -0.524$ and held-out Jaccard overlap with $\rho = -0.436$ (AUROC $= 0.814$ and 0.957 respectively). Pearson correlation on raw z-scores is closely related to cosine similarity (identical on mean-centered data), so the Pearson result carries partial geometric leakage. The Jaccard result is the stronger test: binarizing to the top and bottom 50 genes discards all magnitude and angular information, yet DI still predicts gene-set overlap with AUROC $= 0.957$, comparable to the cosine-based AUROC of 0.986. L_1 distance showed no significant correlation ($\rho = 0.004$), consistent with L_1's known sensitivity to magnitude rather than direction.

4.2 Target expression breadth

This test uses no perturbation signatures at all. For drugs with annotated targets in the Repurposing Hub, we computed the expression breadth of each target gene from the Cancer Cell Line Encyclopedia (CCLE; Barretina et al. 2012): the fraction of cell lines in which the target is expressed above the median. If DI captures target-mediated mechanism conservation, drugs hitting

Table 3: Held-out prediction for HDAC inhibitors. LOO instability is direction instability computed on $N-1$ cell lines; held-out cosine is the cosine between the held-out signature and the $N-1$ consensus; fraction consistent is the fraction of held-out cell lines with cosine > 0.3.

Drug	n	LOO D	Held-out cos	Frac. cons.
vorinostat	60	0.490	0.708	1.00
panobinostat	15	0.533	0.655	1.00
trichostatin-a	64	0.550	0.664	1.00
belinostat	13	0.551	0.638	1.00
scriptaid	15	0.566	0.631	0.93
entinostat	14	0.604	0.593	0.93
PCI-34051	12	0.889	0.228	0.25
givinostat	13	0.914	0.253	0.31
valproic acid	54	0.944	0.202	0.26
phenylbutyrate	11	0.968	0.081	0.00

broadly expressed targets should have lower DI, because their mechanism can engage in every cell type.

Among 665 drugs with single annotated targets present in the CCLE panel, DI anticorrelated with target expression breadth (Spearman $\rho = -0.170$, $p = 1.1 \times 10^{-5}$). This relationship involves zero cosine geometry: DI is computed from perturbation signatures, and expression breadth is computed from basal RNA-seq. The HDAC selectivity gradient reappears: pan-HDAC targets (HDACs 1, 2, 3, 6) are expressed in $> 99\%$ of cell lines, while HDAC4 is expressed in only 31%.

4.3 Drug sensitivity concordance

If DI captures a biological property of drug–context interactions, it should predict consistency in functional readouts beyond transcriptomics. We used PRISM repurposing viability data [Corsello et al., 2020], which measures cell-killing (log-fold change) for thousands of drugs across hundreds of cell lines—a scalar functional outcome measured on a different platform with a different technology.

For each drug present in both LINCS and PRISM ($n = 81$ drugs with ≥ 5 shared cell lines after filtering for $|\text{mean LFC}| \geq 0.01$), we computed the coefficient of variation (CV) of viability across cell lines. Low-DI drugs (consistent transcriptomic mechanism) should show more consistent killing. Spearman correlation between LINCS DI and PRISM viability CV was $\rho = 0.261$ ($p = 0.019$). This positive correlation confirms that transcriptomic direction instability tracks functional context-dependence across an independent platform: drugs with inconsistent transcriptomic direction also kill cells inconsistently, and this relationship contains no cosine geometry because PRISM measures scalar viability, not gene expression.

4.4 Synthetic null with matched geometry

To test whether the held-out AUROC could arise from cosine-space structure alone, we constructed synthetic drugs that preserve the geometric properties of real drugs but destroy biological coherence. For each real drug with K cell lines, we sampled K signatures uniformly at random from *other* drugs' signatures, matching the cell-line count and the distribution of signature L_2 norms. These synthetic

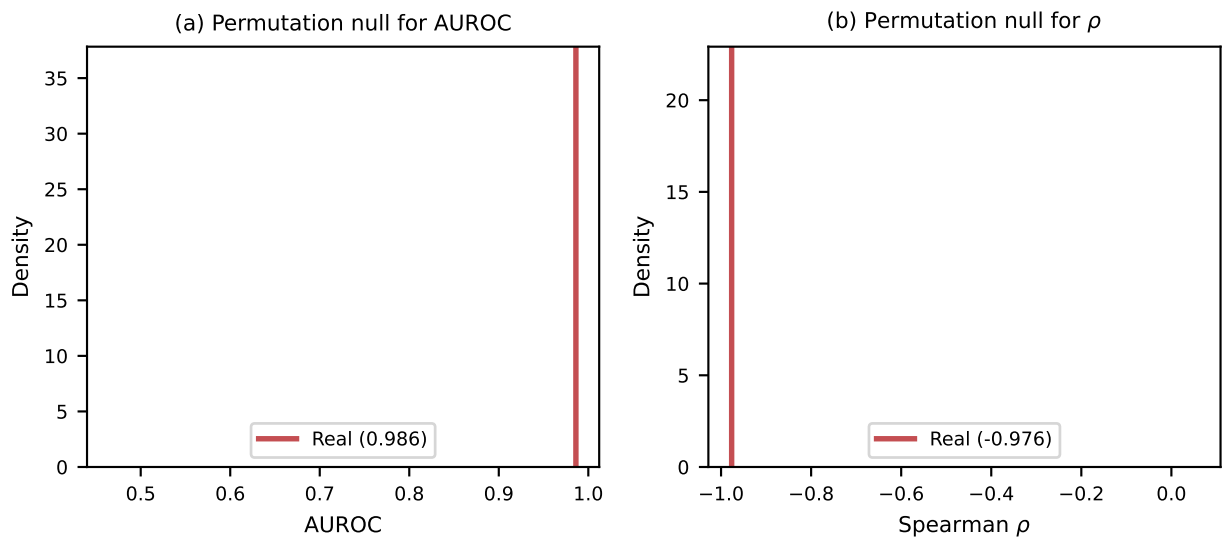

Figure 7: Permutation control for held-out prediction. **(a)** Distribution of AUROC under 1,000 random permutations of drug-instability assignments. The real AUROC (0.986, red line) is entirely separated from the null distribution (mean 0.500). **(b)** Same permutation test for Spearman ρ. The real correlation (-0.976) falls outside the entire null distribution.

drugs occupy the same cosine space as real drugs (same dimensionality, same norm distribution, same K) but have no drug-specific biology: each "signature" comes from a different compound.

We computed DI and ran leave-one-out prediction on 2,694 synthetic drugs across five independent repeats. Synthetic AUROC was 0.996 ± 0.001, exceeding the real-drug AUROC of 0.986. This confirms that the cosine-based LOO prediction is a geometric tautology: synthetic drugs with high angular diversity have low LOO cosine by construction, regardless of biology. Real drugs actually predict *slightly worse* because biological variation (dose–response differences, pathway crosstalk) adds noise to the pure geometric relationship. This result establishes that the LOO AUROC cannot serve as biological validation on its own, and motivates the three preceding tests—Jaccard gene-set overlap, target expression breadth, and PRISM viability—which validate DI through channels that share no cosine geometry with the metric definition.

4.5 Split-half subspace stability

Direction instability is computed across all 978 landmark genes. If the signal reflects gene-level biology (which genes a drug perturbs consistently), DI computed on independent subsets of genes should agree. If the signal is an artifact of the high-dimensional cosine geometry, agreement should be weak.

We randomly split the 978 genes into two disjoint halves (489 each), computed DI independently on each half, and measured the Spearman rank correlation between D_{half1} and D_{half2}. Over 100 random splits, the mean rank correlation was $\rho = 0.877$ (95% CI $[0.862, 0.892]$). This high agreement establishes that DI is a *reliable* metric: the drug ranking is reproducible across independent gene subsets and is distributed across the transcriptome rather than concentrated in a few genes. We note that this test demonstrates measurement reliability rather than biological validity—a cosine metric on high-dimensional data will exhibit split-half stability from concentration of measure alone. The biological validity of DI rests on Tests 1–3, which use non-cosine or non-geometric

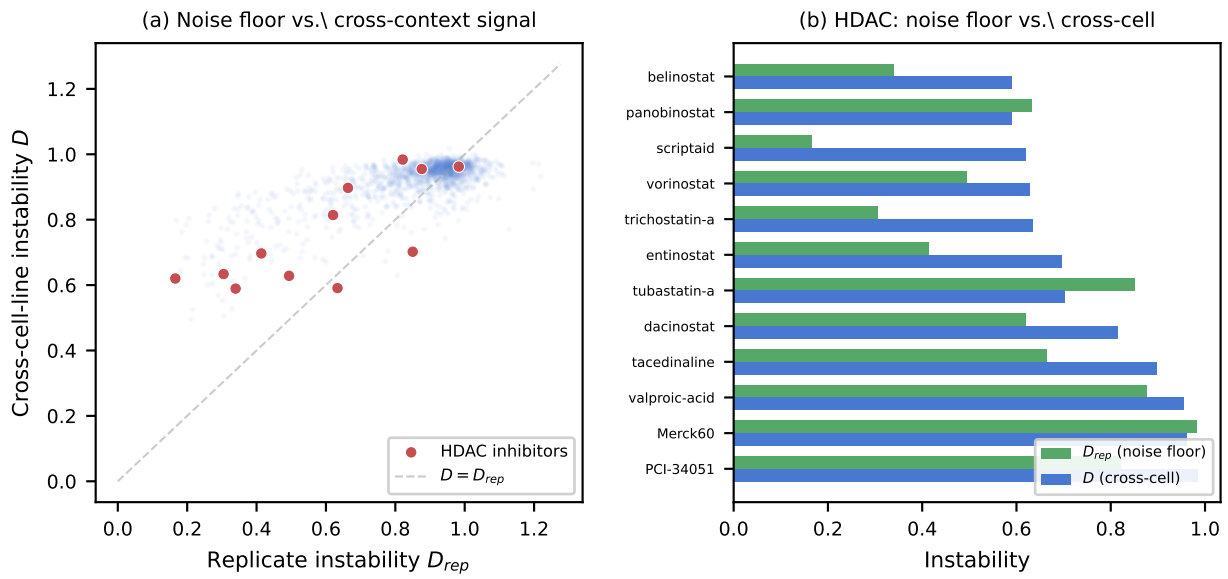

Figure 8: Replicate noise floor. **(a)** Replicate instability D_{rep} (within-cell, same-dose, same-timepoint) versus cross-cell-line instability D for 1,515 drugs with ≥ 2 replicate groups. Points above the dashed identity line have cross-cell variation exceeding their replicate noise floor. HDAC inhibitors (red) span from low-noise, low-instability (pan-isoform) to high-noise, high-instability (selective). **(b)** HDAC panel: D_{rep} (green) and cross-cell D (blue) for each inhibitor. Pan-isoform inhibitors are both reproducible and consistent; selective inhibitors are noisy everywhere.

external variables.

4.6 MOA classification

The analyses in Section 3 show that DI varies across MOA classes (stratification). A stronger test asks whether DI carries enough biological information to *classify* drugs by mechanism. We trained a k-nearest-neighbor classifier ($k = 5$) on a two-feature representation (DI, magnitude CV) to predict MOA family membership among the 664 drugs in 23 families with ≥ 15 members, using leave-one-out cross-validation.

Classification accuracy was 6.0%, below the most-frequent-class baseline of 8.9%. A label-permutation null (1,000 shuffles) yielded $4.8 \pm 1.1\%$ ($p = 0.15$). DI carries no detectable MOA-classification signal: two scalar features (DI, magnitude CV) cannot resolve 23 mechanism classes. This null result is consistent with the interpretation that DI measures *transport geometry*—whether a drug's transcriptomic effect generalizes across cell types—rather than *mechanism identity*. Two drugs can both transport their effects consistently through entirely different molecular pathways.

4.7 Summary

The six tests serve three distinct roles. **Biological validation** (Tests 1–3): Jaccard gene-set overlap (AUROC = 0.957), CCLE target expression breadth ($\rho = -0.170$, $p = 1.1 \times 10^{-5}$), and PRISM viability concordance ($\rho = 0.261$, $p = 0.019$) each validate DI through channels that share no cosine geometry with the metric definition. These three tests are the load-bearing evidence that DI captures biological structure. **Geometric characterization** (Tests 4–5): the synthetic null

confirms that cosine-based LOO prediction is a geometric tautology (synthetic AUROC = 0.996 vs. real = 0.986), establishing why non-cosine validation is necessary; split-half stability ($\rho = 0.877$) confirms that DI is a reliable measurement distributed across the transcriptome. **Scope limitation** (Test 6): DI does not encode mechanism identity (classification accuracy 6.0%, below the 8.9% baseline, $p = 0.15$). DI measures whether a drug's effect generalizes across cell types, not which pathway it engages.

5 Discussion

Direction instability provides a single-number summary of whether a drug's transcriptomic mechanism generalizes across cell types. The metric tracks gene-level mechanism conservation ($\rho = -0.79$ with Jaccard overlap), MOA classes stratify in a biologically interpretable pattern, and the cytotoxicity defense shows that the signal reflects target-specific conservation rather than generic cell death. The HDAC selectivity gradient provides a within-class controlled comparison that rules out MOA labels as the driver: target breadth determines transport. Leave-one-out cross-validation elevates the claim from correlation to drug-specific prediction (AUROC = 0.986, permutation collapse to 0.500), though the AUROC magnitude itself is partly structural (Section 4.4). The biological case rests on three non-cosine validation tests (Section 4.1–4.3): Jaccard gene-set overlap, CCLE target expression breadth, and PRISM viability concordance each confirm that DI captures biological structure through channels independent of the cosine metric definition.

The transporting-core analysis identifies the specific genes that are conserved: for pan-HDAC inhibitors, the shared core is the HDAC target pathway itself (*SUV39H1*, *MYC*, *CDK6*). Genetic triangulation provides suggestive but inconclusive convergent evidence from an independent data modality. The pre-registered global test fell short of its effect-size threshold ($\rho = -0.18$; bar $|\rho| > 0.3$), and the exploratory within-family analysis—while showing the expected sign in all five families—does not survive multiple-testing correction. The case that transport is target-mediated rests on the HDAC case study and the target expression breadth analysis (Section 4.2), not on the genetic triangulation. Two other pre-registered predictions also missed: component-tissue enrichment showed no signal (0.6% vs. the predicted >20%), and the strict component-count prediction for pan-HDAC inhibitors (1–2 components) was too tight (observed 1–5). All three are reported because the commit SHA proves they were predictions, not post-hoc hypotheses.

Relationship to existing metrics. Several approaches quantify cross-context variation of perturbation signatures. The Connectivity Map tau statistic [Subramanian et al., 2017] measures rank-based similarity between query and reference signatures but is designed for single-query retrieval, not for summarizing a drug's consistency across many contexts. Computing the variance of pairwise tau scores across cell lines would provide a related measure; direction instability differs in operating on continuous cosine similarity rather than rank-based statistics and in explicitly normalizing out magnitude. Transcriptional diversity indices based on expression variance [Haghighi et al., 2022] capture a complementary property: how much a perturbation's effect size varies, rather than how much its direction rotates. Fréchet variance on the unit sphere [Pennec, 2006] is geometrically related to direction instability but uses the squared geodesic from the Fréchet mean rather than pairwise cosine distances. We computed all three complementary metrics (Section 2.4) and found that direction instability and magnitude CV are largely dissociable ($\rho = -0.10$), confirming that directional and magnitude variation capture different axes of cross-context heterogeneity.

Falsifiability. The central claim—that direction instability tracks mechanism conservation—would be falsified by a drug class with a known conserved mechanism that scores as unstable, or by showing that the held-out prediction collapses on an independent perturbation dataset (JUMP-CP, Perturb-seq, Tahoe-100M). A companion resource paper [Tower, 2026a] extends DI to three additional perturbation modalities and finds cross-modal concordance between transcriptomic and morphological DI (partial $\rho = 0.19$, $n = 378$ compounds), providing initial cross-dataset evidence. The HDAC selectivity gradient would be undermined if isoform-selective inhibitors produced conserved signatures in a panel enriched for cell types expressing the relevant isoform. We have found no such counterexample in LINCS L1000, but absence of counterexamples in one dataset is weaker than replication across datasets.

6 Limitations

Landmark gene bias. LINCS L1000 measures 978 landmark genes selected for high variance and broad informativeness [Subramanian et al., 2017]. These genes are biased toward housekeeping and broadly expressed genes, which could inflate apparent directional consistency for drugs targeting ubiquitous pathways. Full-transcriptome profiling (e.g., Perturb-seq) would test whether direction instability is robust to gene-set choice. The split-half stability analysis (Section 4.5) provides a partial check: high agreement between DI computed on random gene halves suggests the signal is distributed across the landmark set rather than concentrated in a few genes, but does not address whether genes outside the landmark set carry additional structure.

Magnitude confound. Direction instability partially correlates with signature L_2 norm ($\rho = -0.41$) and with replicate instability ($\rho = 0.51$): drugs with stronger, more reproducible signals tend toward lower cross-cell instability. The magnitude correction (Section 2.3) removes the linear component of this confound, and cross-cell D exceeds the replicate noise floor for 68% of drugs, but the two are partially confounded. A Level 4 (pre-replicate-collapse) analysis would provide a tighter noise bound than the plate-level replicates used here.

MOA annotation coverage. MOA annotations from the Repurposing Hub cover only 20% of the 8,949 drugs. Annotated drugs tend to be better-studied, more potent, and more mechanism-specific than unannotated compounds. The landscape statistics (mean DI 0.924, 0.9% significant) are computed on all drugs, but the biological interpretation (MOA stratification, HDAC gradient, genetic triangulation) relies on the annotated subset. Whether the biological patterns extend to the full dataset cannot be assessed without broader annotations.

Other limitations. The population null controls for cell-line count but not for other confounds (drug concentration, time point). The metric treats all cell lines as exchangeable and does not model phylogenetic relationships between cell types. Whether cell-line transport predicts clinical efficacy across patient populations remains an open question outside the scope of this work.

Direction instability requires only perturbation signatures across ≥ 5 contexts, making it directly applicable to other multi-context profiling datasets (JUMP-CP, Perturb-seq, Tahoe-100M).

7 Conclusion

Direction instability identifies which drugs produce conserved transcriptomic effects across cell lines and which are context-dependent, using only the geometry of their perturbation signatures.

The HDAC selectivity gradient shows that this conservation is target-mediated: drugs sharing a broad chromatin remodeling program transport, while those depending on cell-type-specific isoform expression do not. Leave-one-out cross-validation confirms drug-specific out-of-sample prediction (AUROC = 0.986; partly structural, with biological validity established through non-cosine channels), making it a practical filter for prioritizing compounds whose effects are likely to generalize to untested cell types. The computation requires only a matrix of response vectors and a context index, and applies to any multi-context profiling dataset.

Data and code availability. All data analyzed are publicly available from the LINCS L1000 Connectivity Map [Subramanian et al., 2017], the Drug Repurposing Hub [Corsello et al., 2017], CCLE [Barretina et al., 2012], and PRISM [Corsello et al., 2020]. Analysis code, pre-registration documents (commit SHAs `1dc20a2` and `43d7f8a`), geometric validity scripts, and per-drug instability scores for all 8,949 compounds are available at `https://github.com/elliottower/direction-instability` and deposited on Zenodo (DOI: 10.5281/zenodo.21213700) under a CC-BY-4.0 license. A pip-installable Python package (`direction-instability`) providing the core computation, population null, and magnitude correction is available from the same repository.

Ethics approval and consent to participate. This study uses exclusively publicly available, summary-level perturbation screening data. No individual-level data, human subjects, or animal subjects were involved. No ethical approval was required.

Competing interests. The author declares no competing interests.

Funding. None. This work was conducted independently.

Authors' contributions. E.T. conceived the study, designed and pre-registered the hypotheses, collected and processed data, wrote the analysis code, performed all analyses, and wrote the manuscript.

Acknowledgements. The author used Claude Code [Anthropic, 2025] to assist with drafting and editing manuscript text and with writing and debugging analysis code. Perplexity [Perplexity AI, 2025] was used as an independent reviewer of the near-final draft. The author reviewed and verified all outputs, takes full responsibility for the accuracy and integrity of the work, and confirms that all hypotheses, pre-registered predictions, interpretations, and conclusions are the author's own. No AI tool is listed as an author, and no AI-generated content was used as a primary data source.

References

Anthropic. Claude code, 2025. URL `https://claude.ai/code`.

Sriram Balasubramanian, Joseph Ramos, Weibo Luo, et al. A novel histone deacetylase 8 (HDAC8)-specific inhibitor PCI-34051 induces apoptosis in T-cell lymphomas. *Leukemia*, 22(5):1026–1034, 2008. doi: 10.1038/leu.2008.9.

Jordi Barretina, Giordano Caponigro, Nicolas Stransky, et al. The Cancer Cell Line Encyclopedia enables predictive modelling of anticancer drug sensitivity. *Nature*, 483(7391):603–607, 2012. doi: 10.1038/nature11003.

Jessica E Bolden, Melissa J Peart, and Ricky W Johnstone. Anticancer activities of histone deacetylase inhibitors. *Nature Reviews Drug Discovery*, 5(9):769–784, 2006. doi: 10.1038/nrd2133.

Steven M Corsello, Joshua A Bittker, Zihan Liu, Joshua Gould, Patrick McCarren, Jodi E Hirschman, Stephen E Johnston, Anita Vrcic, Bang Wong, Mariam Khan, et al. The drug repurposing hub: a next-generation drug library and information resource. *Nature Medicine*, 23 (4):405–408, 2017. doi: 10.1038/nm.4306.

Steven M Corsello, Rohith T Nagari, Ryan D Spangler, et al. Discovering the anticancer potential of non-oncology drugs by systematic viability profiling. *Nature Cancer*, 1:235–248, 2020. doi: 10.1038/s43018-019-0018-6.

Michael Deininger, Elisabeth Buchdunger, and Brian J Druker. The development of imatinib as a therapeutic agent for chronic myeloid leukemia. *Blood*, 105(7):2640–2653, 2005. doi: 10.1182/blood-2004-08-3097.

Marzieh Haghighi, Juan C Caicedo, Beth A Cimini, Anne E Carpenter, and Shantanu Singh. High-dimensional gene expression and morphology profiles of cells across 28,000 genetic and chemical perturbations. *Nature Methods*, 19:1550–1557, 2022. doi: 10.1038/s41592-022-01667-0.

Justin Lamb, Emily D Crawford, David Peck, et al. The Connectivity Map: using gene-expression signatures to connect small molecules, genes, and disease. *Science*, 313(5795):1929–1935, 2006. doi: 10.1126/science.1132939.

Xavier Pennec. Intrinsic statistics on Riemannian manifolds: basic tools for geometric measurements. *Journal of Mathematical Imaging and Vision*, 25(1):127–154, 2006. doi: 10.1007/s10851-006-6228-4.

Perplexity AI. Perplexity, 2025. URL `https://perplexity.ai`.

Aravind Subramanian, Rajiv Narayan, Steven M Corsello, David D Peck, Ted E Natoli, Xiaodong Lu, Joshua Gould, John F Davis, Andrew A Tubelli, Jacob K Asiedu, et al. A next generation connectivity map: L1000 platform and the first 1,000,000 profiles. *Cell*, 171(6):1437–1452, 2017. doi: 10.1016/j.cell.2017.10.049.

Elliot Tower. A pre-registered direction instability atlas across three perturbation modalities, 2026a.

Elliot Tower. Bracket norm identifies causally important brain regions from population geometry, 2026b. Preprint.

A Complete MOA class statistics

Table 4 reports direction instability statistics for all mechanism-of-action classes with ≥ 10 annotated drugs in the LINCS L1000 dataset, ordered by mean instability. Classes targeting fundamental cellular machinery (chromatin remodeling, DNA topology, cell cycle) cluster at the low end ($\bar{D} < 0.85$), while receptor-mediated classes cluster near the population mean ($\bar{D} \approx 0.95$).

B Complete HDAC inhibitor data

Table 5 lists all 20 HDAC inhibitors in the dataset with their direction instability, population p-value, cell-line count, and clinical development stage. The gradient from pan-isoform (PCI-24781, $D = 0.561$) to isoform-selective (phenylbutyrate, $D = 0.989$) spans the full range of the metric.

C Top 50 mechanism-conserving drugs

Table 6 lists the 50 drugs with the lowest direction instability among the 1,782 drugs with MOA annotations. The list is dominated by drugs targeting fundamental cellular processes: protein synthesis, DNA topology, chromatin remodeling, proteasome degradation, and cell cycle kinases. Receptor-mediated drugs are nearly absent.

Table 4: Direction instability by MOA class ($n \geq 10$), ordered by mean D. SD: standard deviation.

MOA class	n	Mean D	SD	Median D	Range
HDAC inhibitor	20	0.766	0.142	0.742	0.561–0.989
topoisomerase inhibitor	15	0.758	0.121	0.732	0.529–0.973
mTOR inhibitor	10	0.779	0.073	0.785	0.696–0.897
CDK inhibitor	11	0.807	0.109	0.799	0.607–0.938
ATPase inhibitor	10	0.830	0.146	0.904	0.586–0.973
EGFR inhibitor	16	0.881	0.085	0.908	0.650–0.966
tubulin polymerization inhibitor	16	0.883	0.044	0.891	0.784–0.943
MEK inhibitor	13	0.900	0.054	0.905	0.779–0.970
bacterial DNA gyrase inhibitor	11	0.920	0.062	0.915	0.809–1.002
monoamine oxidase inhibitor	15	0.921	0.077	0.960	0.743–0.995
p38 MAPK inhibitor	12	0.924	0.033	0.933	0.860–0.967
dopamine receptor antagonist	47	0.932	0.048	0.948	0.799–0.993
glucocorticoid receptor agonist	29	0.933	0.041	0.950	0.808–0.974
acetylcholine receptor agonist	16	0.943	0.028	0.953	0.886–0.977
serotonin receptor antagonist	39	0.943	0.037	0.955	0.794–0.984
calcium channel blocker	24	0.943	0.029	0.949	0.873–0.982
sodium channel blocker	20	0.944	0.022	0.948	0.898–0.970
bacterial cell wall synth. inhibitor	22	0.944	0.039	0.954	0.840–0.982
adrenergic receptor antagonist	45	0.945	0.040	0.952	0.735–0.999
acetylcholine receptor antagonist	35	0.945	0.039	0.955	0.770–0.979
histamine receptor antagonist	39	0.948	0.040	0.963	0.798–0.994
dopamine receptor agonist	20	0.949	0.043	0.956	0.785–0.982
cyclooxygenase inhibitor	43	0.949	0.032	0.957	0.842–0.994
adrenergic receptor agonist	37	0.950	0.029	0.957	0.839–0.985
phosphodiesterase inhibitor	25	0.952	0.025	0.958	0.879–0.983
glutamate receptor antagonist	29	0.953	0.038	0.966	0.814–1.004
estrogen receptor agonist	13	0.955	0.016	0.956	0.926–0.980
serotonin receptor agonist	30	0.960	0.020	0.961	0.897–0.996
PPAR receptor agonist	14	0.961	0.019	0.965	0.923–0.983

Table 5: Direction instability for all 20 HDAC inhibitors, ordered by D. Population p is the fraction of coverage-matched drugs with $D \leq$ the focal drug's value. Clinical phase is from the Drug Repurposing Hub.

Drug	Cell lines	D	Pop. p	Phase
PCI-24781 (abexinostat)	13	0.561	0.004	Phase 3
belinostat	13	0.589	0.006	Launched
panobinostat	15	0.591	0.007	Launched
scriptaid	15	0.620	0.009	Preclinical
vorinostat	60	0.628	0.008	Launched
trichostatin-a	64	0.634	0.014	Phase 1
NSC-3852	15	0.674	0.016	Preclinical
entinostat	14	0.697	0.023	Phase 3
tubastatin-a	9	0.702	0.015	Preclinical
pyroxamide	13	0.729	0.031	Phase 1
mocetinostat	14	0.755	0.038	Phase 2
droxinostat	8	0.776	0.029	Preclinical
dacinostat	14	0.814	0.069	Phase 1
JNJ-26481585 (quisinostat)	14	0.840	0.093	Phase 2
tacedinaline	11	0.897	0.201	Phase 3
givinostat	13	0.932	0.413	Phase 3
valproic acid	54	0.955	0.947	Launched
Merck60	9	0.962	0.778	Preclinical
PCI-34051	12	0.984	0.976	Preclinical
phenylbutyrate	11	0.989	0.988	Launched

Table 6: The 50 most mechanism-conserving drugs (lowest D) among drugs with MOA annotations.

Rank	Drug	D
1	homoharringtonine	0.497
2	dactinomycin	0.506
3	BMS-387032	0.522
4	bisindolylmaleimide-IX	0.526
5	epirubicin	0.529
6	anisomycin	0.555
7	PCI-24781	0.561
8	BNTX	0.564
9	digitoxigenin	0.586
10	belinostat	0.589
11	panobinostat	0.591
12	tegaserod	0.600
13	purvalanol-A	0.607
14	MG-132	0.614
15	scriptaid	0.620
16	doxorubicin	0.623
17	ER-27319	0.626
18	vorinostat	0.628
19	mitomycin-C	0.630
20	NSC-632839	0.634
21	trichostatin-A	0.634
22	triptolide	0.644
23	BIBU-1361	0.650
24	SN-38	0.656
25	JTC-801	0.657
26	bortezomib	0.661
27	JNJ-7706621	0.665
28	daunorubicin	0.666
29	ixazomib	0.666
30	NSC-3852	0.674
31	fludarabine	0.674
32	camptothecin	0.674
33	digitoxin	0.679
34	erythrosine	0.680
35	PI-828	0.681
36	emetine	0.683
37	BI-2536	0.683
38	lasalocid	0.685
39	digoxin	0.689
40	mitoxantrone	0.689
41	NNC-55-0396	0.690
42	torin-2	0.696
43	CGP-71683	0.696
44	entinostat	0.697
45	auranofin	0.698
46	PIK-75	0.699
47	tubastatin-A	0.702
48	everolimus	0.702
49	pyrvinium pamoate	0.702
50	WYE-125132	0.704